Organic & Biomolecular Chemistry

Cite this: *Org. Biomol. Chem.*, 2012, **10**, 2594

www.rsc.org/obc

PAPER

The mode of binding ACMA–DNA relies on the base-pair nature

Natalia Busto,[a] Begoña García,*[a] José M. Leal,[a] Fernando Secco[b] and Marcella Venturini[b]

Received 9th November 2011, Accepted 10th January 2012
DOI: 10.1039/c2ob06889c

A thermodynamic and kinetic study on the mode of binding of 9-amino-6-chloro-2-methoxi-acridine (ACMA) to poly(dA–dT)·poly(dA–dT) and poly(dG–dC)·poly(dG–dC) has been undertaken at pH = 7.0 and I = 0.1 M. The spectrophotometric, kinetic (T-jump), circular dichroism, viscometric and calorimetric information gathered point to formation of a fully intercalated ACMA complex with poly(dA–dT)·poly (dA–dT) and another one only partially intercalated (7%) with poly(dG–dC)·poly(dG–dC). The ACMA affinity with the A–T bases was higher than with the G–C bases. The two polynucleotide sequences give rise to external complexes when the ACMA concentration is raised, namely, the electrostatic complex poly(dA–dT)·poly(dA–dT)–ACMA and the major groove binding complex poly(dG–dC)·poly(dG–dC)–ACMA. A considerable quenching effect of the ACMA fluorescence is observed with poly(dA–dT)·poly (dA–dT), ascribable to face-to-face location in the intercalated A–T–ACMA base-pairs. The even stronger effect observed in the presence of poly(dG–dC)·poly(dG–dC) is related to the guanine residue from on- and off-slot ACMA positions.

1. Introduction

The recognized biological activity of acridine derivatives as mutagens, antimicrobial, antimalarial or bactericide agents[1] confirms these compounds with a prominent role as antitumour DNA-intercalating drugs.[2] The fluorescent acridine ACMA (Scheme 1) is monocationic under physiological conditions.[3,4] The observed fluorescence properties turn ACMA into an efficient probe to assess the transmembrane ΔpH[5,6] related to the ATPase activity or the proton flux across vesicles.[7] Also from a photophysical standpoint ACMA is an attractive species; its fluorescence behaviour upon intercalating into DNA has been studied earlier.[8–10]

The behaviour of ACMA toward DNA contrasts with that of the acridine proflavine, whose stacking with the DNA bases results in fluorescence enhancement.[11] ACMA has been shown recently to form three different complex species with Calf Thymus (CT)-DNA,[12] which differ from each other by the mode and extent of interaction. CT-DNA is extremely heterogenic both compositionally and structurally; hence, in principle it should not be discarded that the different modes of binding bear relation with the different structural or compositional domains (*e.g.*, AT-rich *vs*. GC-rich), which may display different affinity with the drug.

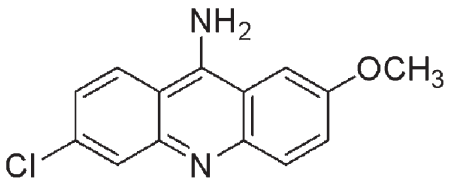

Scheme 1 The ACMA structure (9-amino-6-chloro-2-methoxy acridine).

On the other hand, some authors have concluded that the fluorescence of excited ACMA is not quenched by the adenine, thymine or cytosine nucleobases; instead, it becomes strongly quenched by the guanine residue, well known to be the most oxidizable nucleobase.[8] Photoexcited ACMA is used as an electron acceptor, and guanine as an electron donor. When ACMA and guanine stack up, the decay lifetime considerably decreases; therefore, by means of ACMA–DNA conjugates the electron donor and acceptor sites can be lodged face-to-face in a particular DNA helix sequence.[8–10]

However, our recent fluorescence ACMA titrations with poly (dA–dT)·poly(dA–dT) have revealed a pronounced quenching of the ACMA fluorescence by the A–T bases; also the observed strong quenching of ACMA in the presence of poly(dG–dC)·poly(dG–dC) may occur from nonintercalating interaction.[12] These findings have prompted us to extend the study of the poly (dA–dT)·poly(dA–dT)–ACMA and poly(dG–dC)·poly(dG–dC)–ACMA systems. In this work, we have evaluated the binding of ACMA to poly(dA–dT)·poly(dA–dT) and poly(dG–dC)·poly (dG–dC), its selectivity for a particular sequence and the

[a]*Departamento de Química, Universidad de Burgos, 09001 Burgos, Spain. E-mail: begar@ubu.es*
[b]*Dipartimento di Chimica e Chimica Industriale, Università di Pisa, 56126 Pisa, Italy*

quenching effect, drawing new conclusions regarding the affinity for the A–T and G–C sequences as well as the effect exerted by these bases and the type of binding on the ACMA fluorescence.

2. Experimental

2.1 Materials

Poly(dA–dT)·poly(dA–dT) and poly(dG–dC)·poly(dG–dC) were purchased from Sigma-Aldrich as lyophilized sodium salts, and were used without further purification. Stock solutions of the polynucleotides were prepared by dissolving the solid in water and standardised spectrophotometrically using ε = 13 300 M^{-1} cm^{-1} (λ = 260 nm) for poly(dA–dT)·poly(dA–dT) and ε = 16 800 M^{-1} cm^{-1} (λ = 254 nm) for poly(dG–dC)·poly(dG–dC).[13] The polynucleotide concentration, C_P, was expressed as molarity of base-pairs (M_{BP}). Stock solutions were kept in the dark at 4 °C.

ACMA was purchased from Sigma Aldrich and used without further purification. Stock solutions were prepared by dissolving weighed amounts of the solid in DMSO and kept in the dark at 4 °C. The DMSO content of the aqueous solutions was below 2%. The ACMA molar concentration is denoted as C_D. The aqueous solutions were prepared with doubly distilled, deionised water (Millipore Q apparatus, APS, Los Angeles, California). The ionic strength was adjusted using sodium chloride. Sodium cacodylate, $(CH_3)_2AsO_2Na$, was employed as a buffer to keep constant the medium acidity at pH 7.0.

2.2 Methods

The pH measurements were performed using a Metrohm 16 DMS Titrino pH-meter fitted out with a combined glass electrode and a 3 M KCl solution as a liquid junction. The fluorescence experiments were performed with a Shimadzu Corporation RF-5301PC spectrofluorometer (Duisburg, Germany) at λ_{exc} = 419 nm and λ_{em} = 477 nm. The titrations were carried out by adding increasing amounts of the polynucleotide (up to $C_D = 1.5 \times 10^{-6}$ M) to the cell with the dye solution. The quenching experiments with the poly(dA–dT)·poly(dA–dT)–ACMA and poly(dG–dC)·poly(dG–dC)–ACMA systems were performed at 0.0, 0.1, 0.3 and 0.6 C_D/C_P ratios, using sodium iodide as a quencher.

The thermal behaviour of the poly(dA–dT)·poly(dA–dT)–ACMA and poly(dG–dC)·poly(dG–dC)–ACMA systems was studied by differential scanning calorimetry (DSC) using a Nano DSC Instrument (TA, Waters LLC, New Castle, USA). To reduce the bubble formation to a minimum upon heating, the reference and the sample solutions were degassed prior to loading into the DSC cells and afterwards a 5 atm pressure was applied. The samples were scanned from 20 to 130 °C at 1 °C min^{-1} scan rate for the poly(dG–dC)·poly(dG–dC)–ACMA system and from 20 to 90 °C at 1 °C min^{-1} scan rate for the poly(dA–dT)·poly(dA–dT)–ACMA system.

Circular dichroism (CD) spectra were recorded on a MOS-450 Bio-Logic dichrograph (Claix, France). The measurements were performed in 1.0 cm path-length cells at 25 °C; the titrations were carried out by injecting increasing micro amounts of the dye into a known volume of the polymer solution.

Viscosity measurements were performed on an Ubbelodhe viscometer (Schott, Mainz, Germany) immersed in a water-bath at 25.0 ± 0.1 °C. The flow time was assessed with a digital stopwatch; the sample viscosity was averaged out from triplicated measurements. To estimate the change of the solvent viscosity induced by DMSO, micro amounts of DMSO (33%) were added to 3 ml solvent samples up to 2% DMSO. The data obtained showed a coherent increase in viscosity (η_{DMSO}) with a rise in the DMSO content. The viscosity of solutions containing different DMSO amounts and a constant polynucleotide amount, η_{poly} were measured by adding increasing DMSO micro amounts (33%) to 3 ml of the polynucleotide 2.27×10^{-4} M, up to 2% DMSO, at pH 7.0, I = 0.1 M and 25 °C. Finally, the viscosity of the polynucleotide–ACMA mixtures ($\eta_{poly-ACMA}$) was measured by adding increasing ACMA amounts to the polynucleotide solution. The relative viscosity was calculated using the expression: $\eta/\eta_0 = (\eta_{poly-ACMA} - \eta_{DMSO})/(\eta_{poly} - \eta_{DMSO})$. The η/η_0 ratio is related to the relative polynucleotide length by the relationship:[14]

$$L/L_0 = (\eta/\eta_0)^{1/3}$$

The kinetic measurements were performed on a T-jump apparatus built up in our laboratory on the basis of the Rigler *et al.* prototype.[15] The instrument is equipped with a tungsten lamp–monochromator system as the light source and is able to measure fluorescence and absorbance changes. The kinetic curves recorded in the fluorescence mode were collected on an Agilent (Santa Clara, CA) 54622A oscilloscope, transferred to a PC and evaluated with the Table Curve program of the Jandel Scientific package (AISN software, Richmond, CA). The time constants were averaged out from at least ten kinetic runs, the observed spread being 10%.

3. Results

3.1 Equilibria

Fig. 1 shows the emission spectra of ACMA, whose intensity decreased upon adding poly(dA–dT)·poly(dA–dT) and poly(dG–dC)·poly(dG–dC); this effect was sharper for the latter due to

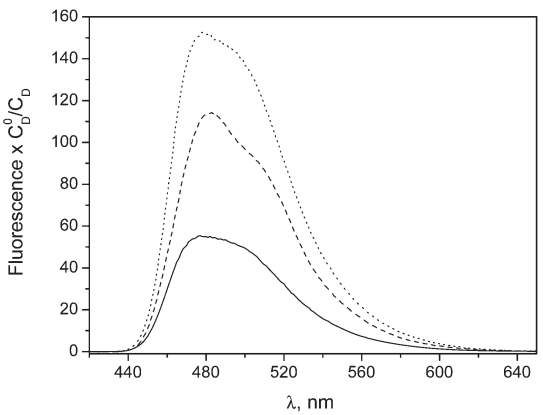

Fig. 1 Fluorescence spectra recorded of ACMA alone (dotted line), poly(dA–dT)·poly(dA–dT)–ACMA (dashed line) and poly(dG–dC)·poly(dG–dC)–ACMA (solid line) at C_D/C_P = 0.1. C_D^0 = 1.50 μM, pH 7.0, I = 0.1 M (NaCl), T = 25 °C, λ_{exc} = 419 nm and λ_{em} = 477 nm.

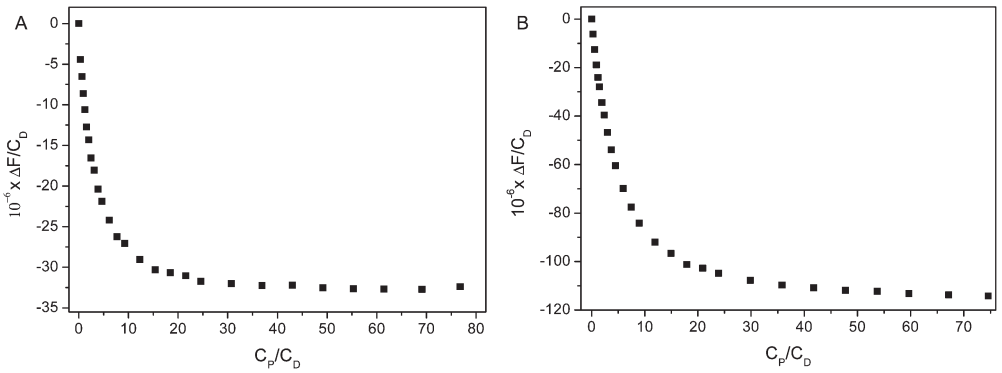

Fig. 2 Fluorescence binding isotherms for (A) poly(dA–dT)·poly(dA–dT)–ACMA, and (B) poly(dG–dC)·poly(dG–dC)–ACMA systems at C_D^0 = 1.50 μM, pH = 7.0, I = 0.1 M (NaCl), T = 25 °C, λ_{exc} = 419 nm and λ_{em} = 477 nm.

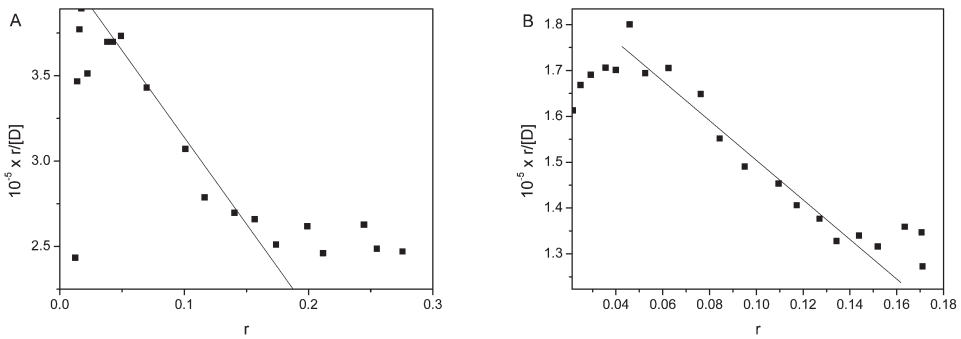

Fig. 3 Scatchard plot (eqn (3)) for (A) poly(dA–dT)·poly(dA–dT)–ACMA and (B) poly(dG–dC)·poly(dG–dC)–ACMA systems at C_D^0 = 1.50 μM, pH = 7.0, I = 0.1 M (NaCl), T = 25 °C, λ_{exc} = 419 nm and λ_{em} = 477 nm.

dye-base interaction. The binding of ACMA to the investigated DNAs can be represented by the apparent reaction (eqn 1),

$$P + D \underset{}{\overset{K}{\rightleftharpoons}} PD \quad (1)$$

where D and PD stand for the free and the bound ACMA, and P represents the polynucleotide free sites. The binding constants of the poly(dA–dT)·poly(dA–dT)–ACMA and poly(dG–dC)·poly(dG–dC)–ACMA systems were evaluated by fluorescence titrations; the binding isotherms were monophasic in both cases (Fig. 2), and the fluorescence decreased sharply after addition of each polynucleotide.

The apparent equilibrium constant of reaction (1) is expressed by eqn (2),

$$K = \frac{[PD]}{[P] \times [D]} \quad (2)$$

Evaluation of the K constant requires introducing the site size value, n, the number of base-pairs occupied by a drug unit upon binding.[16] A Scatchard-type analysis of the data-pairs has enabled us to evaluate the parameter n according to eqn (3),

$$\frac{r}{[D]} = K_{SC}(B - r) \quad (3)$$

where the parameter B is associated with the site size by the relationship $n = (1 + 1/B)/2$.[16] The concentration ratio $r = [PD]/C_P$ was evaluated from $[PD] = \Delta F/\Delta\phi$, being $\Delta F = F - F_0$ and $\Delta\phi = \phi_{PD} - \phi_D$.[17] Fig. 3 shows the measured data plotted according to eqn (3). The observed scattered data-pairs is characteristic of the Scatchard analysis; to this aim, only the stretch with negative slope is involved in the fitting. Once the site size was determined, the equilibrium constant is evaluated with eqn (4), assuming that the free site concentration, [P], on the polymer lattice is expressed according to:[16,17] $[P] = C_P \times f(r)$, being $f(r) = [1 - nr]^n \times [1 - (n - 1)r]^{n-1}$.

The binding constant, K, and $\Delta\phi$ were obtained from the $C_D/\Delta F$ *vs.* 1/[P] fitting (Fig. 4) according to:

$$\frac{C_D}{\Delta F} = \frac{1}{\Delta\phi} + \frac{1}{K\,\Delta\phi} \times \frac{1}{[P]} \quad (4)$$

As the initial value of [P] was unknown, an iteration procedure was applied replacing [P] by C_P in eqn (4). The $\Delta\phi$ value obtained was then used to re-evaluate r, and the procedure was iterated until the convergence was achieved after only few steps. Table 1 lists the n and K values deduced.

3.2 Kinetics

The kinetic experiments were performed by shifting the equilibrium on the basis of the T-jump relaxation method. All the relaxation curves recorded for both systems were monoexponential (Fig. 5), that is, only a single relaxation effect was observed. The plot (Fig. 6) of the reciprocal of the relaxation time, $1/\tau$, *vs.*

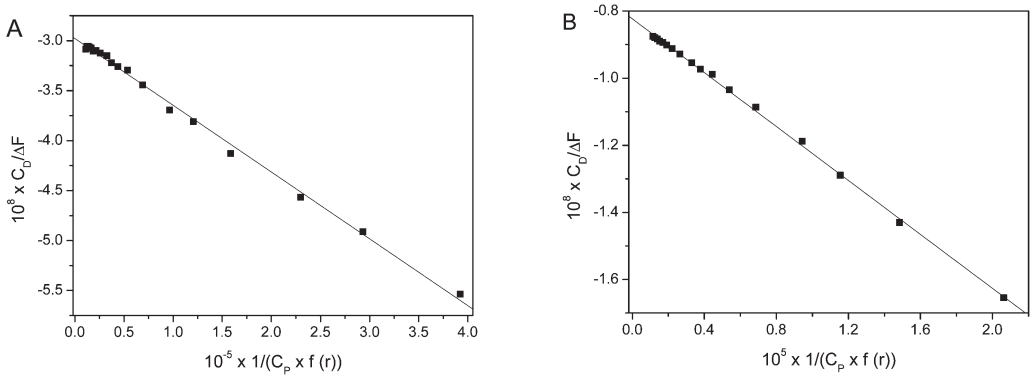

Fig. 4 Fitting of eqn (4) to the spectrofluorimetric titration data-pairs for (A) the poly(dA–dT)·poly(dA–dT)–ACMA, and (B) the poly(dG–dC)·poly(dG–dC)–ACMA systems at C_D^0 = 1.50 μM, pH = 7.0, I = 0.1 M (NaCl), T = 25 °C, λ_{exc} = 419 nm and λ_{em} = 477 nm.

Table 1 Binding constant (K) and site size (n) for poly(dA–dT)·poly(dA–dT)–ACMA poly(dG–dC)·poly(dG–dC)–ACMA and CT–DNA–ACMA systems. I = 0.1 M (NaCl), T = 25 °C

	n^a	10^{-5} K $(M^{-1})^b$	10^{-7} k_f $(M^{-1}$ $s^{-1})^c$	10^{-2} k_d $(s^{-1})^c$	10^{-5} k_f/k_d
poly(dA–dT)·poly(dA–dT)–ACMA	2.1	4.00 ± 0.17	6.10 ± 0.01	1.17 ± 0.07	5.21 ± 0.14
poly(dG–dC)·poly(dG–dC)–ACMA	1.7	2.00 ± 0.02	2.90 ± 0.07	2.37 ± 0.39	1.22 ± 0.17
CT–DNA–ACMA[d]	1.7	1.73 ± 0.01	2.94 ± 0.07	4.54 ± 0.66	0.65 ± 0.11

[a] From eqn (3). [b] From eqn (4). [c] From eqn (5). [d] From ref. 12.

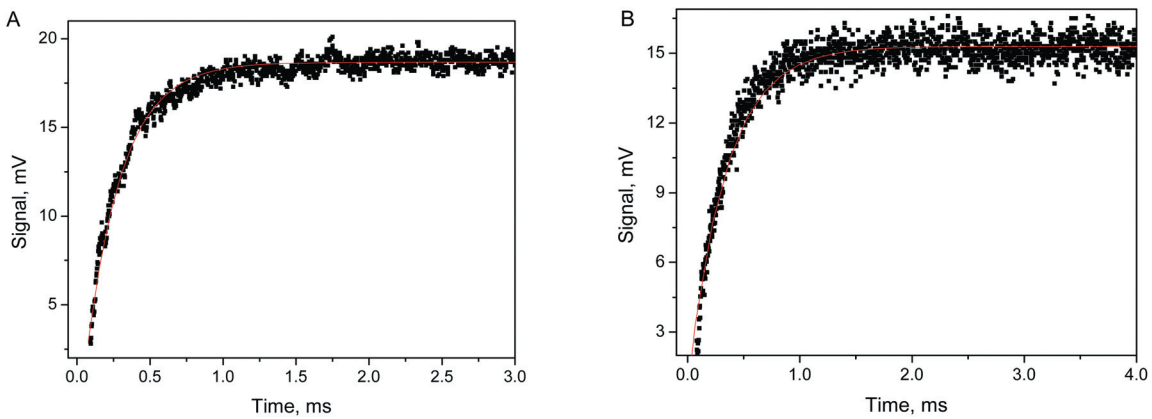

Fig. 5 T-jump relaxation curves recorded in the fluorescence mode for (A) poly(dA–dT)·poly(dA–dT)–ACMA, C_D = 1.02 × 10^{-5} M and C_P = 9.96 × 10^{-5} M, and (B) poly(dG–dC)·poly(dG–dC)–ACMA systems, C_D = 1.39 × 10^{-5} M and C_P = 1.20 × 10^{-4} M at pH = 7.0, I = 0.1 M, T = 25 °C, λ_{exc} = 420 nm and λ_{em} = 480 nm.

the reactants concentration term, [P] + [D], nicely fulfiled eqn (5),

$$\frac{1}{\tau} = k_f([D] + [P]) + k_d \quad (5)$$

where k_f and k_d represent the forward and backward rate constants, respectively, of the apparent reaction (1). The k_f, k_d and K = k_f/k_d values are listed in Table 1.

3.3 Circular dichroism

CD measurements contribute to elucidate the mode of binding of drugs to nucleic acids. Even though ACMA is achiral in nature, its interaction with DNA induces changes in the CD spectra of the resulting complex. Fig. 7 shows the CD spectra of poly(dA–dT)·poly(dA–dT) and poly(dG–dC)·poly(dG–dC) with rising ACMA amounts. The negative and positive bands of poly (dA–dT)·poly(dA–dT) at 245 and 265 nm (Fig. 7A) shifted 10 nm to red and increased in intensity in the course of the stepwise titration, showing a neat isodichroic point at 268 nm. In addition, the negative band of poly(dG–dC)·poly(dG–dC) at 250 nm (Fig. 7B) shifted 4 nm to blue and decreased in intensity, while the intensity of the positive band at 270 nm rose and shifted 8 nm to red. In both cases, an induced circular dichroism effect appeared at 343 nm with a new band due to ACMA addition; this band has also been reported in the presence of

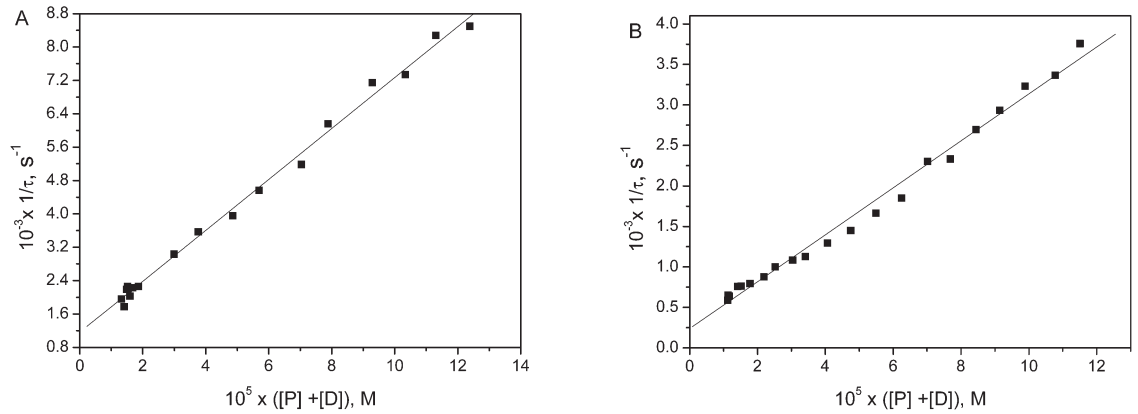

Fig. 6 Variation of $1/\tau$ *vs.* ([P] + [D]) (eqn (5)) for (A) poly(dA–dT)·poly(dA–dT)–ACMA, and (B) poly(dG–dC)·poly(dG–dC)–ACMA systems at pH = 7.0, I = 0.1 M, T = 25 °C.

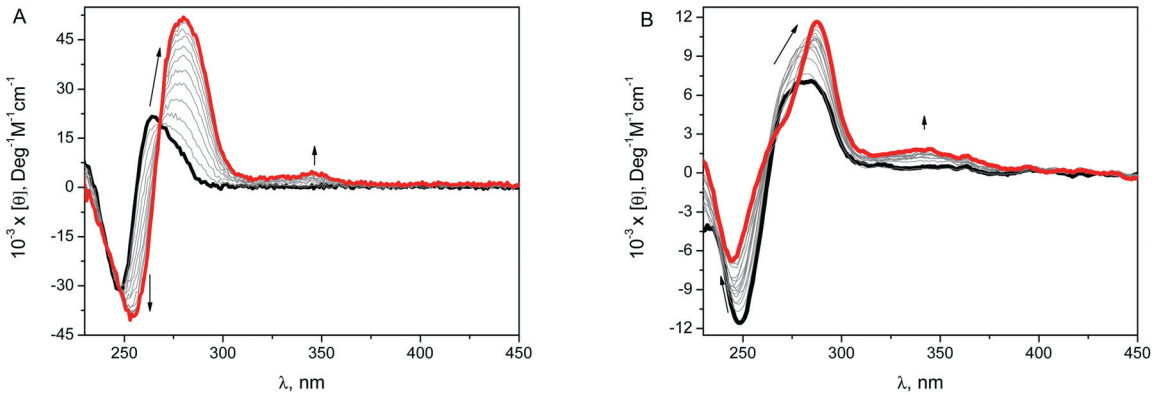

Fig. 7 CD spectra of (A) poly(dA–dT)·poly(dA–dT)–ACMA system C_P^0 = 24.5 μM, and (B) poly(dG–dC)·poly(dG–dC)–ACMA system C_P^0 = 50.0 μM. C_D/C_P from 0 to 1.1 (arrow sense), pH = 7.0, I = 0.1 M (NaCl), and T = 25 °C.

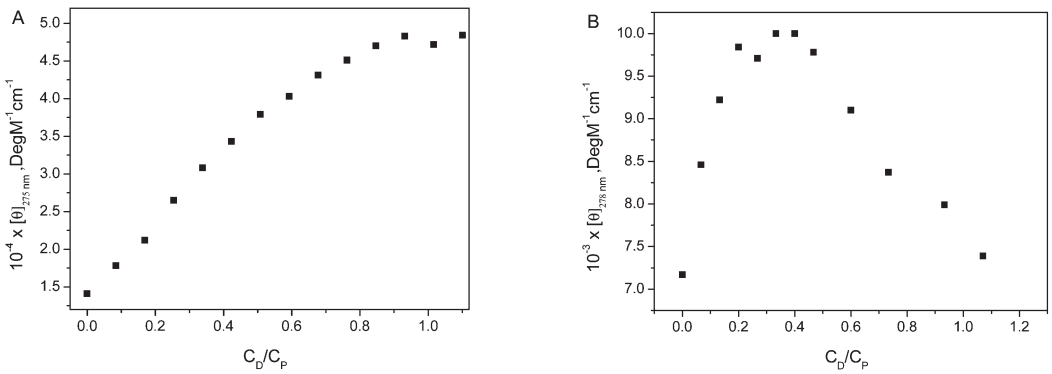

Fig. 8 Molar ellipticity *vs.* C_D/C_P ratio at pH = 7.0, I = 0.1 M (NaCl), T = 25 °C and C_D/C_P from 0 to 1.1. (A) poly(dA–dT)·poly(dA–dT)–ACMA system at λ = 275 nm, C_P^0 = 24.5 μM, and (B) poly(dG–dC)·poly(dG–dC)–ACMA system at λ = 278 nm, C_P^0 = 50.0 μM.

CT–DNA.[12] Fig. 8 plots the change of the molar ellipticity as a function of the C_D/C_P ratio for both systems.

3.4 Viscosity

Viscosity is an efficient tool to detect the ability of small molecules to affect the DNA contour length;[14] the binding is accompanied by an increase in viscosity that reflects the polymer lengthening. The relative viscosity for poly(dA–dT)·poly(dA–dT)–ACMA rose in the $0 \leq C_D/C_P \leq 0.2$ range, reaching a plateau (Fig. 9). For poly(dG–dC)·poly(dG–dC)–ACMA, however, viscosity showed a more complex profile, suggesting the occurrence of more than a simple binding process.

3.5 Quenching

Quenching experiments can shed light into the location of a fluorescent molecule bound to a polynucleotide. The information

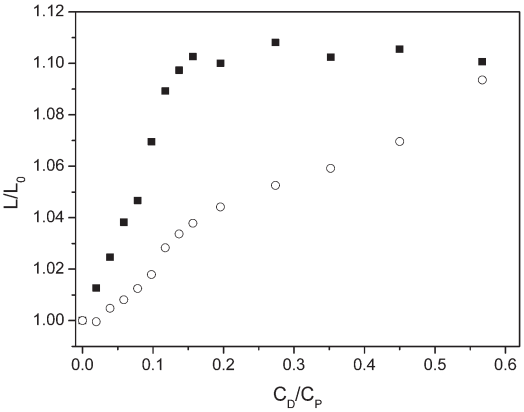

Fig. 9 Relative viscosity of the poly(dA–dT)·poly(dA–dT)–ACMA (■) and poly(dG–dC)· poly(dG–dC)–ACMA (○) systems: C_P^0 = 22.7 mM, pH = 7.0, I = 0.1 M (NaCl) and T = 25 °C.

deduced from exposure to the quencher has helped us to decide whether the ligand is located outside or inside the double helix. To reliably compare the behaviour of the poly(dA–dT)·poly(dA–dT)–ACMA and poly(dG–dC)·poly(dG–dC)–ACMA systems with that of CT–DNA,[12] three fluorescence quenching experiments were performed at 0.1, 0.3 and 0.6 C_D/C_P ratio on each one of the systems, sodium iodide being the quencher. An additional comparative experiment was carried out with ACMA alone. The Stern–Volmer plots[18] obtained for ACMA alone, poly(dG–dC)·poly(dG–dC)–ACMA at 0.3 and 0.6 C_D/C_P ratio and poly(dA–dT)·poly(dA–dT)–ACMA at C_D/C_P = 0.1 were all linear (Fig. 10). By contrast, poly(dA–dT)·poly(dA–dT)–ACMA at 0.3 and 0.6 C_D/C_P ratio showed a clear downward curve (Fig. 10A), whereas poly(dG–dC)·poly(dG–dC)–ACMA displayed only a modest curvature at C_D/C_P = 0.1 (Fig. 10B). The downward curve of the Stern–Volmer plot unveils the existence of a fluorophore fraction accessible to the quencher and another fraction inaccessible. This feature can be accounted for by the modified Stern–Volmer equation:[18]

$$\frac{F_0}{F_0 - F} = \frac{1}{f_a K_a [Q]} + \frac{1}{f_a} \qquad (6)$$

where f_a stands for the accessible fraction, K_a is the Stern–Volmer quenching constant of the accessible fraction, and $[Q] = C_{NaI}$, that is, f_a indicates the nonintercalated ACMA fraction to the double helix and $(1 - f_a)$ the on-slot fraction. Fig. 11 shows the $F_0/\Delta F$ *vs.* $1/C_{NaI}$ plot of the poly(dA–dT)·poly(dA–dT)–ACMA system at 0.3 and 0.6 C_D/C_P ratio. The straight line plot, eqn (6), nicely fitted the data pairs, yielding the quenching parameters.

The Stern–Volmer plots for free ACMA and poly(dA–dT)·poly(dA–dT)–ACMA at C_D/C_P = 0.1 (Fig. 10A) yielded the values $K_a = 196 \pm 0.6\ M^{-1}$ and $10\ M^{-1}$, respectively.

Therefore, a pronounced diminution of K_a implies that ACMA is in fact fully intercalated into the polymer. As the C_D/C_P ratio was raised, the Stern–Volmer plot became nonlinear (Fig. 10A), and application of eqn (6) yielded f_a = 57% and K_a = 102 at C_D/C_P = 0.3 and f_a = 80% and K_a = 121 at C_D/C_P = 0.6 (Fig. 11). For poly(dG–dC)·poly(dG–dC)–ACMA, the off-slot fluorophore fraction accessible to the quencher is f_a = 93% at C_D/C_P = 0.1, with K_a = 156. Actually, at C_D/C_P = 0.3 and 0.6, the resulting quenching effect was close to that observed for free ACMA (Fig. 10B).

3.6 Thermal stability of poly(dA–dT)·poly(dA–dT)–ACMA and poly(dG–dC)·poly(dG–dC)–ACMA. Differential scanning calorimetry

The melting process was investigated by DSC over the $0 \leq C_D/C_P \leq 0.6$ concentration range by plotting the heat flow as a function of temperature in the presence of increasing ACMA amounts. DSC measurements provide the melting temperature, T_m, from double to single strand, defined as the midpoint through the melting transition. The associated changes in the calorimetric enthalpy, ΔH_{cal}, and entropy, ΔS_{cal}, were evaluated by integration of the areas enclosed by the C_P–T and (C_P/T)–T transition curves, respectively, and the pre/post-transition baseline; C_{Pd} and C_{Ps} denote the heat capacity of the double and single strands, respectively, and ΔC_P the difference between C_{Pd} and C_{Ps} at the melting temperature.

Fig. 12 shows the DSC curves for the polynucleotide alone and at 0.1, 0.3 and 0.6 C_D/C_P ratio. The melting transition relies on the C_D/C_P ratio, reaching higher melting temperature as the

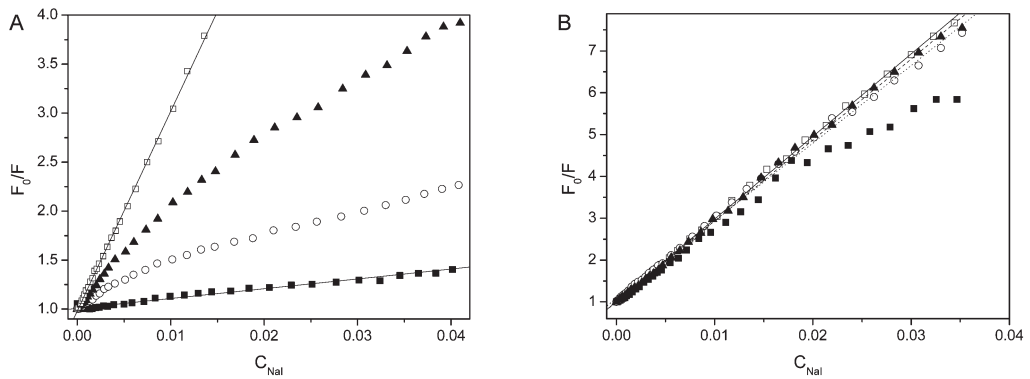

Fig. 10 Stern–Volmer plot for (A) poly(dA–dT)·poly(dA–dT)–ACMA, and (B) poly(dG–dC)·poly(dG–dC)–ACMA: (□) free ACMA at $C_D^0 = 3.1 \times 10^{-5}$ M, (▲) C_D/C_P = 0.6, (○) C_D/C_P = 0.3 and (■) C_D/C_P = 0.1 at $C_D^0 = 2.6 \times 10^{-6}$ M, pH = 7.0, I = 0.1M, T = 25 °C, λ_{exc} = 419 nm and λ_{em} = 477 nm.

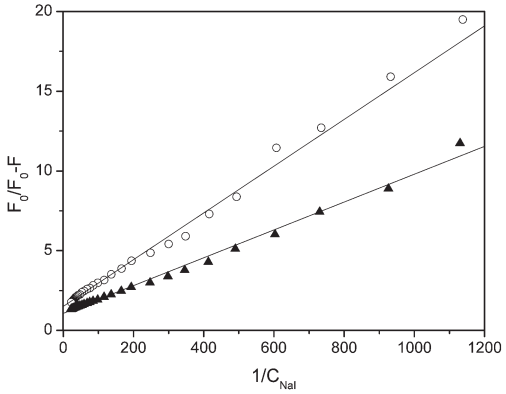

Fig. 11 Modified Stern–Volmer plot, eqn (6), for the poly(dA–dT)·poly(dA–dT)–ACMA system, (○) C_D/C_P = 0.3 and (▲) C_D/C_P = 0.6. $C_D^0 = 2.6 \times 10^{-6}$ M, pH = 7.0, I = 0.1M, T = 25 °C, λ_{exc} = 419 nm and λ_{em} = 477 nm.

C_D/C_P ratio was raised. Table 2 lists the thermodynamic parameters derived.

4. Discussion

The binding constants, K, deduced (Table 1) reveal stronger ACMA affinity for the A–T bases; the closeness of the static and dynamic outcome supports the reliability of the values obtained. The binding constant for both systems was 6 and 3 times higher than the values obtained, respectively, for poly(dA–dT)·poly(dA–dT)–proflavine and poly(dG–dC)·poly(dG–dC)–proflavine under the same conditions,[19] whereas 9-aminoacridine[20] and acriflavine[21] manifest higher affinity for poly(dG–dC)·poly(dG–dC) indicating that, being these drugs acridines, they behave differently from one another.

Fig. 2 shows the fluorescence spectra of free ACMA and ACMA bound to A–T and G–C. Free ACMA and the poly(dG–dC)·poly(dG–dC)–ACMA system present two partially overlapped emission bands, with maxima at 477 and 500 nm; the similarity of the bands indicates that the fluorophore is mostly located outside the double helix. For poly(dA–dT)·poly(dA–dT)–ACMA, the two maxima shifted 6 nm to red, suggesting possible intercalation.[22] Such difference between the binding modes is corroborated by other techniques. The observed effect of the ACMA quenching with both the A–T and G–C sequences contrasts with the assertion[8–10] that only the guanine nucleobase was found to quench the ACMA fluorescence when both species pile up.

The quenching experiments recorded in the presence of NaI reveal quite a different behaviour. For poly(dG–dC)·poly(dG–dC)–ACMA at C_D/C_P = 0.1, ACMA is only partially intercalated (7%) into the duplex. At C_D/C_P = 0.3 and 0.6, the observed quenching resembles that of free ACMA (Fig. 10A), revealing that actually 100% of the ACMA bound to the G–C base-pairs is

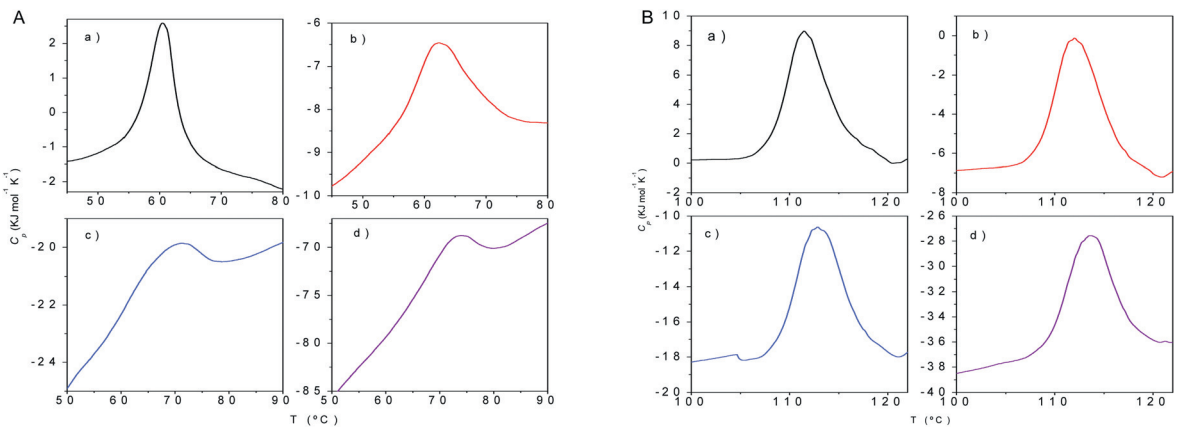

Fig. 12 DSC curves. poly(dA–dT)·poly(dA–dT)–ACMA system (A) and poly(dG–dC)·poly(dG–dC)–ACMA system (B) at pH 7.0, I = 0.1M and P = 5 atm. a) C_D/C_P = 0, b) C_D/C_P = 0.1, c) C_D/C_P = 0.3 and d) C_D/C_P = 0.6.

Table 2 Melting temperature, T_m, enthalpy (ΔH_{cal}) and entropy (ΔS_{cal}), heat capacity of the double (C_{Pd}) and single (C_{Ps}) strands, respectively, and difference between C_{Pd} and C_{Ps} at the melting temperature (ΔC_P) determined from the DSC curves of poly(dA–dT)·poly(dA–dT)–ACMA and poly(dG–dC)·poly(dG–dC)–ACMA at pH = 7.0, I = 0.1 M and P = 5 atm

	C_D/C_P	T_m (°C)	ΔH_{cal} (kJ mol^{-1})	ΔS_{cal} (kJ mol^{-1})	C_{Pd}	C_{Ps}	ΔC_P
poly(dA–dT)·poly(dA–dT)–ACMA	0	60.5	17.2	51.4	−1.3	−1.7	−0.4
	0.1	62.2	12.6	37.4			
	0.3	69.0	8.3	24.4			
	0.6	72.7	15.7	45.4			
poly(dG–dC)·poly(dG–dC)–ACMA	0	111.5	42.1	109.5	0.2	0.0	−0.2
	0.1	112.0	38.7	100.5	−6.8	−7.3	−0.5
	0.3	112.9	39.9	103.2	−18.1	−18.0	0.1
	0.6	113.5	40.8	105.6	−37.6	−36.0	1.7

forming an external complex. For poly(dA–dT)·poly(dA–dT)–ACMA, however, the quenching experiments convey quite a different behaviour (Fig. 10B); at $C_D/C_P = 0.1$, ACMA is in fact fully intercalated into the double helix, as the rather small Stern–Volmer slope ($K_S = 10\ M^{-1}$) reveals. When the C_D/C_P ratio was raised, ACMA became more accessible to the quencher, observing a downward curve. The plot of eqn (6) (Fig. 11) yielded the nonintercalated ACMA fraction exposed to the quencher, that is, some 57% and 80% for $C_D/C_P = 0.3$ and 0.6, respectively. These fractions, though large, are far from the 100% free ACMA exposure, whose linear plot is shown. This observation suggests that either different partially intercalated complexes are formed or new dye units are placed outside the helix once the intercalated complex becomes saturated, thus giving rise to aggregate formation. The latter option will be corroborated below.

The viscosity data also reveal a remarkable difference between the hydrodynamic behaviour of A–T–ACMA and G–C–ACMA. The former displayed a sharp linear η/η_0 *vs.* C_D/C_P plot up to $C_D/C_P \approx 0.17$; within this range, all the available sites become occupied, that is, the site size in the intercalated complex is $n_i \approx 6$. Further ACMA addition has no effect on the relative viscosity because the polynucleotide is already saturated and the external aggregate is formed from the intercalated complex; therefore, it does not affect the double helix, whose elongation remains unaltered, in good agreement with the quenching experiments. The CD experiments (Fig. 8A) indicate that both complexes, intercalated and external, modify the unwinding of the double helix**.** The global site-size $n = 2$ calculated with eqn (3) (Table 1) means that $n_i \approx 6$ for each intercalated ACMA unit, that is, two additional ACMA units must be present in the external aggregate. In other words, although we concluded before that free ACMA forms no aggregates, the presence of A–T bases does, in fact, favour the stacking.

The viscosity experiments have shown that the poly(dG–dC)·poly(dG–dC)–ACMA system yields two different complexes depending on the C_D/C_P ratio. The sigmoid curve observed (Fig. 9) suggests that an external complex is formed, which evolves to a partially intercalated species in the $0.05 \leq C_D/C_P \leq 0.3$ range. Above this ratio, external groove binding is feasible, in accordance with the observed CD inversion of the θ ratio at $C_D/C_P = 0.3$ (Fig. 8B). The sign inversion of the CD bands had already been reported for DNA–proflavine due to the switch from intercalated to groove binding upon adding ethanol;[19] that is, the formation of two distinct complexes (partially intercalated and groove binding), depending on the ACMA content, is also hinted by the CD experiments. Since the electron transfer between the ACMA excited state and the N7 guanine site occurs at the major groove (the place where the N7 site is located) the dye in the G–C–ACMA complex is allocated to the major groove. Since saturation appears at $C_D/C_P \approx 0.3$, the site size of the partially intercalated complex should be $n_i \approx 3$, larger than the global $n = 1.7$ value deduced from Scatchard analyses over a wider concentration range (Table 1). In other words, for each ACMA intercalated unit, another unit must be located in the poly(dG–dC)·poly(dG–dC) groove, most likely forming a dimer. The different modes of binding reported here are also reinforced by the DSC experiments (Fig. 12).

Thermal stabilization of both polynucleotides induced by ACMA addition suggests strong double helix stabilization for A–T ($\Delta T_m = 12$ °C) and weaker for G–C ($\Delta T_m = 2$ °C) within the same 0.0–0.6 C_D/C_P range (Table 2). It is well known that intercalation increases the resistance to denaturation;[23] hence, the stronger intercalation found for A–T–ACMA relative to G–C–ACMA concurs well with the ΔT_m values obtained. The ΔH_{cal} and T_m values deduced for the pure polynucleotides slightly differ from those reported by Tikhomirova *et al.*;[24] to fairly stand comparison, it must be recalled here that these authors gave the properties for mol nucleotide, whereas we refer to base-pairs, as revealed by the absorptivity coefficients used to deduce the proper concentration. In the presence of ACMA, the heat capacity strongly increases, those of the double and the single strand, an effect to be attributed to the ACMA interaction.

It is remarkable that the A–T–ACMA unwinding proceeds with a change in the heat capacity (ΔC_P) that depends on the ACMA content, whereas the slope of the pretransition effect increases. From the shape of the curves it can be surmised that the ACMA dissociation commences prior to the cooperative complex disruption, involving two steps in the temperature-induced change of the complex. The first step is characterized by a stepwise increase of the heat capacity, that is, gradual accumulation of thermal energy by the fluctuating complex structure. The second step represents the highly cooperative complex dissociation with duplex unwinding and breaking of the ACMA aggregates outside the helix, which normally is accompanied by a positive heat effect.[25] Extrapolation of the apparent heat capacity of the pre- and postdenaturation ranges can result in significant uncertainty, because actually it is ignored where the transition starts and where it ends. For this reason, the $\Delta C_P = C_{Pss} - C_{Pds}$ values were not evaluated for the A–T–ACMA system. For this system, ΔH_{cal} and ΔS_{cal} decreased at $C_D/C_P = 0.3$, and increased at $C_D/C_P = 0.6$ (Table 2); such a difference could be related to the stability of the aggregate present as C_D increases, whose disgregation requires energy input. The G–C–ACMA system behaves differently; the ΔH_{cal} and ΔS_{cal} parameters (Table 2) were insensitive to ACMA concentration, meaning that the partially intercalated and groove binding complexes have similar energy. Fig. 12A and B show that ΔC_P is much less for G–C–ACMA than for A–T–ACMA.

The sets of results gathered have shown that the ACMA interaction mechanism with the A–T and G–C sequences could be represented by the equation:

$$P + D \underset{k_d}{\overset{k_f}{\rightleftharpoons}} PD_1 \overset{K_2}{\rightleftharpoons} PD_2$$

where PD_1 stands for the partially intercalated complex and PD_2 for a major groove binding for poly(dG–dC)·poly(dG–dC), whereas PD_1 is a fully intercalated complex and PD_2 an electrostatic external binding for poly(dA–dT)·poly(dA–dT).

Fukui *et al.*[8] had shown that, for DNA consisting of only (dA–dT) base-pairs, the fluorescence decay of single excited ACMA is single exponential, similar to free ACMA, and concluded that the ACMA fluorescence remains unaltered for the A–T sequence. The fluorescence quantum yield for synthesized A–T–ACMA conjugates is 0.65, and 0.66 for free ACMA. However, our results have shown that poly(dA–dT)·poly(dA–dT)

lowers the ACMA fluorescence due to intercalation (Fig. 1 and 2A), whereas the A–T external complex does not influence the fluorescence intensity. Likewise, the fluorescence lifetime of the excited ACMA decreases upon adding guanosine,[8] displaying two fluorescence lifetimes when the guanine residue is adjacent to ACMA. The rate for the forward electron transfer depends on the ACMA–guanine distance, thereby the longer lifetime component comes from the ACMA emission in the off-slot conformation, whereas the shorter one is assigned to the partial on-slot conformation. These findings are in good agreement with the above results, thus underscoring the main features of the two complexes, 7% intercalated (PD_1) and major groove binding (PD_2).

The kinetic experiments for both systems were performed at $C_D/C_P \leq 0.1$ ratio, in which the monoexponential trend reflects the kinetics of intercalation; hence, the k_f/k_d value corresponds to intercalation constant, K_{int}, whereas the global constant deduced from the fluorescence data is $K = K_{int} \times K_2$. Table 1 shows that, for the A–T system, K_{int} is four times larger relative to the G–C system, whereas K_2 turned out to be 0.77 and 1.64, respectively. The rate constants (k_f and k_d) reveal that the PD_1 complex with the A–T bases forms faster and dissociates slower than the G–C complex, concurrent with a higher intercalation degree in poly (dA–dT)·poly(dA–dT). It can then be concluded that ACMA is an intercalating agent with higher affinity for poly(dA–dT)·poly (dA–dT) compared to poly(dG–dC)·poly(dG–dC), in contrast with the behaviour of 9-aminoacridine[20] and acriflavine,[21] which manifest higher affinity for poly(dG–dC)·poly(dG–dC).

Finally, we shall compare the ACMA behaviour with CT-DNA, poly(dA–dT)·poly(dA–dT) and poly(dG–dC)·poly (dG–dC). The three partially intercalated complexes (47%, 15% and 6% on-slot) observed for CT–DNA–ACMA[12] can be convincingly justified by the results obtained. The ACMA intercalation into CT–DNA is mainly due to the A–T fraction, and the units located outside the helix can bind either the major groove of the G–C fraction, or electrostatically to A–T.

Comparison of the thermodynamic constants with those for the formation of the A–T–ACMA, G–C–ACMA and CT–DNA–ACMA complex systems (Table 1), demonstrates that the constants for CT–DNA are much closer to those for G–C relative to A–T. The equilibrium kinetic constant k_f/k_d for CT–DNA–ACMA became 2 and 8 times lower relative to G–C–ACMA and A–T–ACMA, respectively, showing that the affinity depends not only on the DNA composition, but also on structural features. The finding that the k_d dissociation constant of the CT–DNA–ACMA complex is 2 and 4 times greater than those of G–C–ACMA and A–T–ACMA (Table 1) indicates that the ACMA units intercalated into CT–DNA become less retained than into poly(dA–dT)·poly(dA–dT) and poly(dG–dC)·poly(dG–dC), most likely due to the major unwinding of the DNA double helix.

At $C_D/C_P < 0.1$, the on-slot ACMA percentage is 47% into CT–DNA,[12] 7% into G–C, and 100% into A–T (this work). A simple calculation leads one to conclude that CT–DNA consists of 43% A–T and 57% G–C. However, CT–DNA contains (roughly) 42% G–C.[26,27] This finding indicates that the fraction intercalated into DNA is not the average of the intercalation into the A–T and G–C sequences because of the complex structure and composition of CT–DNA.

In summary, we have shown that ACMA interacts with the A–T and G–C bases quite differently; the sets of experiments reported reveal greater affinity and complexity for the former. The photochemical properties of ACMA regarding its interaction with guanine come about in positions different from face-to-face, whereas this position is required to induce the quenching with the A–T base-pairs.

Acknowledgements

The financial support by Ministerio de Educación y Ciencia, Project CTQ2009-13051/BQU, supported by FEDER, Junta de Castilla y León, Projects BU-013A-09 and GR257 and Universidad de Burgos with funding by Caja de Burgos, Spain, is gratefully acknowledged.

References

1 L. R. Ferguson and W. A. Denny, *Mutat. Res., Fundam. Mol. Mech. Mutagen.*, 2007, **623**, 14–23.
2 M. F. Braña, M. Cacho, A. Gradillas, B. de Pascual-Teresa and A. Ramos, *Curr. Pharm. Des.*, 2001, **7**, 1745–1780.
3 A. C. Capomacchia and S. G. Schulman, *Anal. Chim. Acta*, 1975, **77**, 79–85.
4 A. Marty, M. Bourdeaux, M. Dell'Amico and P. Viallet, *Eur. Biophys. J.*, 1986, **13**, 251–257.
5 V. Fregni and R. Casadio, *Biochim. Biophys. Acta, Bioenerg.*, 1993, **1143**, 215–222.
6 R. McCarty, *J. Bioenerg. Biomembr.*, 2006, **38**, 67–74.
7 C. Camarasa, S. Prieto, R. Ros, J. M. Salmon and P. Barre, *Yeast*, 1996, **12**, 1301–1313.
8 K. Fukui, K. Tanaka, M. Fujitsuka, A. Watanabe and O. Ito, *J. Photochem. Photobiol., B*, 1999, **50**, 18–27.
9 S. Hess, W. B. Davis, A. A. Voityuk, N. Rösch, M. E. Michel-Beyerle, N. P. Ernsting, S. A. Kovalenko and J. L. Pérez Lustres, *ChemPhysChem*, 2002, **3**, 452–455.
10 U. Pachmann and R. Rigler, *Exp. Cell Res.*, 1972, **72**, 602–608.
11 *Metal Ions in Biological Chemistry*, R. F. Pasternack and E. J. Gibbs, Marcel Dekker, New York, 1996, vol. 33.
12 N. Busto, B. García, J. M. Leal, J. F. Gaspar, C. Martins, A. Boggioni and F. Secco, *Phys. Chem. Chem. Phys.*, 2011, **13**, 19534–19545.
13 R. D. Wells, J. E. Larson, R. C. Grant, B. E. Shortle and C. R. Cantor, *J. Mol. Biol.*, 1970, **54**, 465–497.
14 G. Cohen and H. Eisenberg, *Biopolymers*, 1969, **8**, 45–55.
15 R. Rigler, C. R. Rabl and T. M. Jovin, *Rev. Sci. Instrum.*, 1974, **45**, 580–588.
16 J. D. McGhee and P. H. von Hippel, *J. Mol. Biol.*, 1974, **86**, 469–489.
17 T. M. Jovin and G. Striker, *Mol. Biol. Biochem. Biophys.*, 1977, **24**, 245–281.
18 *Principles of Fluorescence Spectroscopy*, ed. J. R. Lakowicz and B. R. Masters 2008, vol. 13, pp. 277–330.
19 B. García, J. M. Leal, R. Ruiz, T. Biver, F. Secco and M. Venturini, *J. Phys. Chem. B*, 2010, **114**, 8555–8564.
20 W. R. Wilson, B. C. Baguley, L. P. G. Wakelin and M. J. Waring, *Mol. Pharmacol.*, 1981, **20**, 404–414.
21 L. M. Chan and J. A. McCarter, *Biochim. Biophys. Acta, Nucleic Acids Protein Synth.*, 1970, **204**, 252–254.
22 D. E. V. Schmechel and D. M. Crothers, *Biopolymers*, 1971, **10**, 465–480.
23 D. J. Patel, *Acc. Chem. Res.*, 1979, **12**, 118–125.
24 A. Tikhomirova, N. Taulier and T. V. Chalikian, *J. Am. Chem. Soc.*, 2004, **126**, 16387–16394.
25 *Methods Enzymol.*, ed. G. P. Privalov, P. L. Privalov and G. K. A. Michael L. Johnson, Academic Press, 2000, vol. 323, pp. 31–62.
26 E. Chargaff, C. F. Crampton and R. Lipshitz, *Nature*, 1953, **172**, 289–292.
27 J. Marmur and P. Doty, *J. Mol. Biol.*, 1962, **5**, 109–118.

